Available online at www.sciencedirect.com
ScienceDirect
Trans. Nonferrous Met. Soc. China 30(2020) 2599−2612
Transactions of Nonferrous Metals Society of China
www.tnmsc.cn

Creep aging behavior of retrogression and re-aged 7150 aluminum alloy

Qing WANG[1,2], Li-hua ZHAN[1,2,3], Yong-qian XU[1,2,3], Chun-hui LIU [1,2],
Xing ZHAO[1,2], Ling-zhi XU[1,2], You-liang YANG[1,2], Yi-xian CAI[1,2,3]

1. School of Mechanical and Electrical Engineering, Central South University, Changsha 410083, China;
2. State Key Laboratory of High-Performance Complex Manufacturing,
Central South University, Changsha 410083, China;
3. Light Alloy Research Institute of Central South University, Changsha 410083, China

Received 31 August 2019; accepted 28 May 2020

Abstract: Creep aging behavior of retrogression and re-aged (RRAed) 7150 aluminum alloy (AA7150) was systematically investigated using the creep aging experiments, mechanical properties tests, electrical conductivity tests and transmission electron microscope (TEM) observations. Creep aging results show that the steady-state creep mechanism of RRAed alloys is mainly dislocation climb (stress exponent≈5.8), which is insensitive to the grain interior and boundary precipitates. However, the total creep deformation increases over the re-aging time. In addition, the yield strength and tensile strength of the four RRAed samples are essentially the same after creep aging at 140 °C for 16 h, but the elongation decreases slightly with the re-aging time. What's more, the retrogression and re-aging treatment are beneficial to increase the hardness and electrical conductivity of the creep-aged 7150 aluminum alloy. It can be concluded that the retrogression and re-aging treatment before creep aging forming process can improve the microstructure within grain and at grain boundary, forming efficiency and comprehensive performance of mechanical properties and electrical conductivity of 7150 aluminum alloy.

Key words: creep aging forming; creep behavior; mechanical properties; electrical conductivity; aging precipitates; Al−Zn−Mg−Cu alloy

1 Introduction

Al−Zn−Mg−Cu (7000 series) alloys are extensively used in aircraft components due to their low density and high strength [1,2]. These complex aircraft components are generally manufactured by creep aging forming (CAF), which is a novel metal forming technology to simultaneously shape and strengthen the Al−Zn−Mg−Cu alloys during one-step forming and aging treatment process [3,4]. There are many heat treatment tempers suitable for the 7000 series aluminum alloys, such as T6 (peak aging treatment), T74 (two-stage aging treatment) and T77 (retrogression and re-aging treatments, RRA) tempers. Among them, T77 temper not only maintains the strength of T6 temper, but also keeps high stress corrosion resistance of T74 temper [5,6]. Therefore, the combination of the CAF and the RRA treatment process may be applied to manufacturing large complex components of Al−Zn−Mg−Cu alloys. In order to acquire aircraft components with high performance and high forming efficiency by CAF, it is vitally important to

Foundation item: Project (2017YFB0306300) supported by the National Key Research and Development Program of China; Project (2017ZX04005001) supported by the National Science and Technology Major Project, China; Project (JCKY2014203A001) supported by National Defense Program of China; Projects (51905551, 51675538, 51601060) supported by the National Natural Science Foundation of China; Projects (Kfkt2018-03, zzYJKT2019-11) supported by State Key Laboratory of High-Performance Complex Manufacturing, China
Corresponding author: Li-hua ZHAN; E-mail: yjs-cast@csu.edu.cn
DOI: 10.1016/S1003-6326(20)65405-X

study the creep aging behavior of the retrogression and re-aged Al−Zn−Mg−Cu alloy.

The creep aging behavior of 7000 series aluminum alloys has been studied since CAF technology was proposed. ARABI JESHVAGHANI et al [7,8] investigated the effects of time and temperature on the creep forming of 7075 aluminum alloy, and analyzed the microstructural evolution during creep forming. ZHAN et al [9] carried out CAF experimental studies on 7055 aluminum alloy and explained the hardening mechanism during creep aging process. ZHANG et al [10] studied the effect of deformation degree on the CAF of 7475 aluminum alloy, and expounded heterogeneous matrix nucleation sites introduced during creep aging, which make intragranular precipitates finer and denser than that of stress-free aging. LIN et al [11] discussed evolution of precipitates during two-stage stress−aging of an Al−Zn−Mg−Cu alloy, and elaborated two-stage stress−aging processing which can optimize the distribution of aging precipitates within grain and at grain boundaries. ZHENG et al [12] investigated multi-step stress−relaxation−aging of 7050 aluminum alloy under different pre-strained conditions, and elaborated the interaction between precipitates and dislocation during stress−relaxation−aging. These studies focused on the creep aging behavior of solid solution 7000 series aluminum alloys. In order to improve the formability and comprehensive properties of 7000 series aluminum alloys using CAF process, several other explorations have been carried out. ARABI JESHVAGHANI et al [13] studied the effects of multi-step heat treatments on the CAF of 7075 aluminum alloy to decrease spring-back and exfoliation corrosion susceptibility. LEI et al [14] conducted a research on the effect of initial tempers of creep-aged 7050 aluminum alloy on the microstructures and properties, and found that the precipitates of retrogression temper after creep aging had the less effect on inhibiting the dislocation movement, thus, a larger creep deformation was obtained for retrogression temper than that for the others. Recently, a retrogression and stress−aging (RSA) treatment of Al−Zn−Mg−Cu alloys was investigated for CAF application by XU et al [15]. Compared with the RRA temper, the RSA increased the size of matrix precipitates, narrowed the width of precipitate-free zone (PFZ) and made the grain boundary precipitates more discontinuous for the Al−Zn−Mg−Cu alloy. This showed that the retrogression and re-aged treated Al−Zn−Mg−Cu alloy might be used to acquire aircraft components with high performance by CAF process. However, the creep aging behavior of the RRAed Al−Zn−Mg−Cu alloy is rarely mentioned.

In this work, the creep aging behavior of RRAed 7150 aluminum alloy was studied using a combination of experimental techniques, including creep aging, tensile, electrical conductivity tests and TEM observations. To this end, a typical AA7150 was employed and undergone half-hour retrogression at 190 °C and re-aged at 120 °C for 0, 4, 8 and 24 h, followed by creep aging at 140 °C for 16 h. The creep deformation and mechanism of the four different RRAed AA7150 samples were analyzed. TEM and high resolution TEM (HRTEM) technologies were adopted to characterize the microstructures. In addition, the mechanical properties, hardness and electrical conductivity tests were carried out and discussed. The results show that the RRA temper is more conducive to improve the forming efficiency and comprehensive performance than the retrogression temper for AA7150 CAF application.

2 Experimental

2.1 Materials and heat treatments

The present study was carried out on 7150 commercial aluminum alloy. The composition was Al−6.19Zn−2.22Mg−2.18Cu−0.11Zr (wt.%). The as-received material was a hot-rolled plate with 80 mm in thickness. The creep test samples with the gauge length of 50 mm and thickness of 2 mm were machined along the rolling direction at the surface layer of the hot-rolled plate, and the geometry of the specimen is shown in Fig. 1.

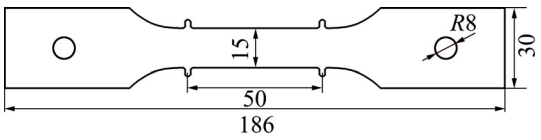

Fig. 1 Geometry and size of specimen (unit: mm)

The scheme of heat treatments used in current study is shown in Fig. 2. In order to simulate the pre-treatment of sheet for creep aging forming application, the samples were solution treated at

470 °C for 60 min, followed by water quenching, 2% pre-stretching, and more than 2 d of natural aging. For the retrogression and re-aging treatments, the samples were aged at 120 °C for 24 h. Retrogression was carried out at 190 °C for 30 min followed by re-aging at 120 °C for four different re-aged time of 0 h (RRAed-0 h), 4 h (RRAed-4 h), 8 h (RRAed-8 h) and 24 h (RRAed-24 h).

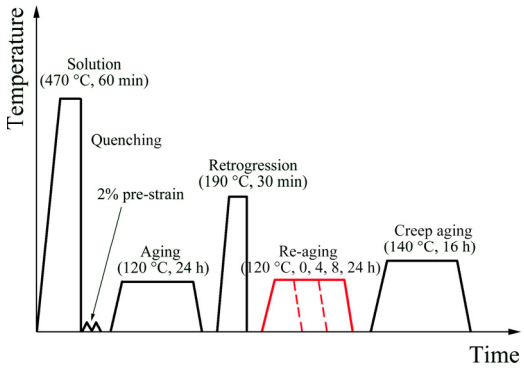

Fig. 2 Scheme of heat treatments used

2.2 Creep aging tests

Considering the effect of aging hardening temperature on the microstructures and properties of 7000 series aluminum alloys, the temperature of 140 °C and aging time of 16 h were chosen for the creep aging tests, whilst the applied stresses were 250, 300 and 350 MPa, respectively. The sample was fitted and aligned in the middle of the machine furnace (SUST-D5, China) and the temperature could be controlled within 2 °C. The target temperature was raised at a heating rate of 5 °C/s and held for 10 min. After that, the load was applied with the loading speed of 15 N/s, and the constant temperature and load were maintained for 16 h. Besides, interruption creep tests (1, 2, 4, 8, and 12 h) were carried out to obtain the Vickers hardness and electrical conductivity evolution of RRAed AA7150 during the creep aging process.

2.3 Tensile, hardness and electrical conductivity tests

The tensile tests were carried out on the MTS CMT5205 machine at a tensile speed of 2 mm/min. Each experiment was repeated at least two times. Vickers hardness tests were conducted on a digital micro-Vickers hardness tester (HuaYin200HVS−5, China) under a load of 500 N for a dwell time of 15 s. Ten measurements were performed for each testing sample to calculate an average value of the hardness. The electrical conductivity measurement was conducted on a Fischer electrical conductivity instrument (SIGMASCOPE® SMP350, Germany). Each test for each sample was repeated at least five times.

2.4 Microstructure characterization

The precipitate microstructure of AA7150 was observed by Tecnai-F20 (200 kV) field-emission-gun transmission electron micro-scope (FEG-TEM). The samples were ground to 60−80 μm, cut into 3 mm-diameter disks, and then twin-jet-electro-polished to perforation with a mixture of 30 vol.% nitric acid and 70 vol.% methanol at −30 °C with a potential of 15 V. The size of grain interior precipitates in TEM images was statistically counted by Nano Measurer 1.2 software, and more than three images (about 300 precipitates) were counted for each sample to obtain average value.

3 Results and discussion

3.1 Creep behaviors of retrogression and re-aged AA7150

Figures 3(a) and (b) respectively show the creep strain and creep strain rate of four different RRAed AA7150 samples under the applied stress of 350 MPa at 140 °C. The creep strain curves were smoothened to eliminate the experimental errors and differentiated with time to calculate the creep strain rate. The primary and steady creep stages can be distinguished by creep strain rate curve. It can be found in Fig. 3 that the creep behaviors of four different RRAed AA7150 samples show both the typical primary and steady creep stages. Steady creep rate and total creep strain of four different RRAed AA7150 samples are shown in Table 1. Three experimental phenomena can be observed: (1) The creep strain of AA7150 increases over re-aging time. After the creep aging for 16 h, the creep strain of RRAed-24h sample is 1.2 times that of RRAed-0h sample; (2) The difference of primary creep stage is the main contribution of the difference of total creep strain; (3) The duration of primary creep stage lasts for about 5 h at RRAed-0 h, 6 h at RRAed-4 h, 8 h at RRAed-8 h, and 9 h at RRAed-24 h samples, respectively. The duration time of the primary creep stage is significantly prolonged with the increase of the re-aging time, which leads to a large creep strain.

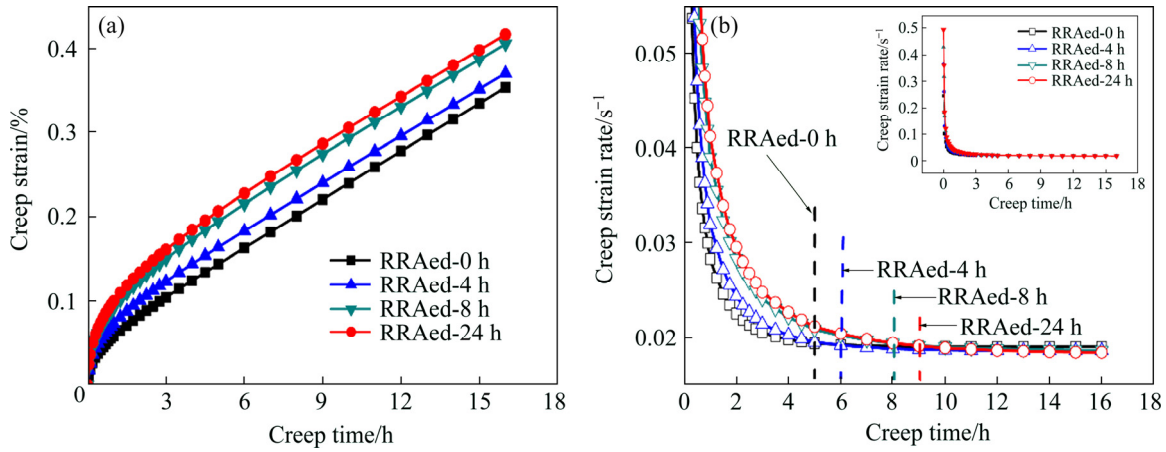

Fig. 3 Creep strain (a) and creep strain rate (b) curves of different RRAed AA7150 samples under 350 MPa at 140 °C

Table 1 Creep behaviors of four different RRAed AA7150 samples under applied stresses of 250, 300 and 350 MPa at 140 °C

Re-aging time/h	250 MPa		300 MPa		350 MPa		Stress exponent
	Steady creep strain rate/s^{-1}	Total creep strain/%	Steady creep strain rate/s^{-1}	Total creep strain/%	Steady creep strain rate/s^{-1}	Total creep strain/%	
0	7.19×10^{-7}	0.0745	1.45×10^{-6}	0.1435	5.30×10^{-6}	0.3535	5.87
4	7.33×10^{-7}	0.0989	1.46×10^{-6}	0.1479	5.22×10^{-6}	0.3702	5.77
8	7.44×10^{-7}	0.1066	1.43×10^{-6}	0.1590	5.35×10^{-6}	0.4053	5.79
24	7.08×10^{-7}	0.1087	1.46×10^{-6}	0.1711	5.34×10^{-6}	0.4166	5.94

The value of stress exponent (n) can be calculated by the slope of the relation curve between $\ln\dot{\varepsilon}$ and $\ln\sigma$ in Fig. 4 to indicate the deformation mechanism of stable creep [16]. A stress exponent about 5.8 is obtained for four different RRAed AA7150 samples, and the specific values are shown in Table 1. The dislocation climb at high temperature leads to the value of n in the range of 4−6 [17]. The stress exponent shows that the creep strains of four different RRAed AA7150 samples are mainly attributed to the dislocation climb mechanism.

3.2 Evolution of mechanical properties and electrical conductivity of RRAed AA7150 during creep aging process

3.2.1 Mechanical properties

Figure 5 shows the hardness evolution of four different RRAed AA7150 samples during the 140 °C and 300 MPa creep aging. The hardness of RRAed-0 h sample increases rapidly at first, reaches its peak value of HV 187 after 4 h creep aging and then tends to be stable. However, the hardnesses of other three RRAed AA7150 samples decrease slightly with the creep aging time. Two possible reasons for the decline of hardness are coarsening of precipitates and re-dissolution of fine precipitates due to high temperature (140 °C) creep aging of the sample re-aged at 120 °C. Generally, the hardness of the aluminum alloy decreases very slowly in the early stage of aging treatment. Therefore, the hardness decrease of creep aged-samples in the early stage of creep aging is mainly attributed to the re-dissolution of fine precipitates.

Figure 6 illustrates the yield strength (YS), ultimate tensile strength (UTS) and elongation of four different RRAed AA7150 samples before (Fig. 6(a)) and after (Fig. 6(b)) creep aging process at 140 °C and 300 MPa. It can be found that the RRAed-0 h sample has the lowest YS, UTS, and elongation from Fig. 6(a). However, the difference between other three RRAed AA7150 samples is not obvious. This indicates that a short time of re-aging treatment can make the AA7150 reach its peak-aged value. It can be seen from Fig. 6(b) that the YS and UTS of four different RRAed AA7150 samples are almost the same after 16 h creep aging process, but the elongation decreases with the increasing

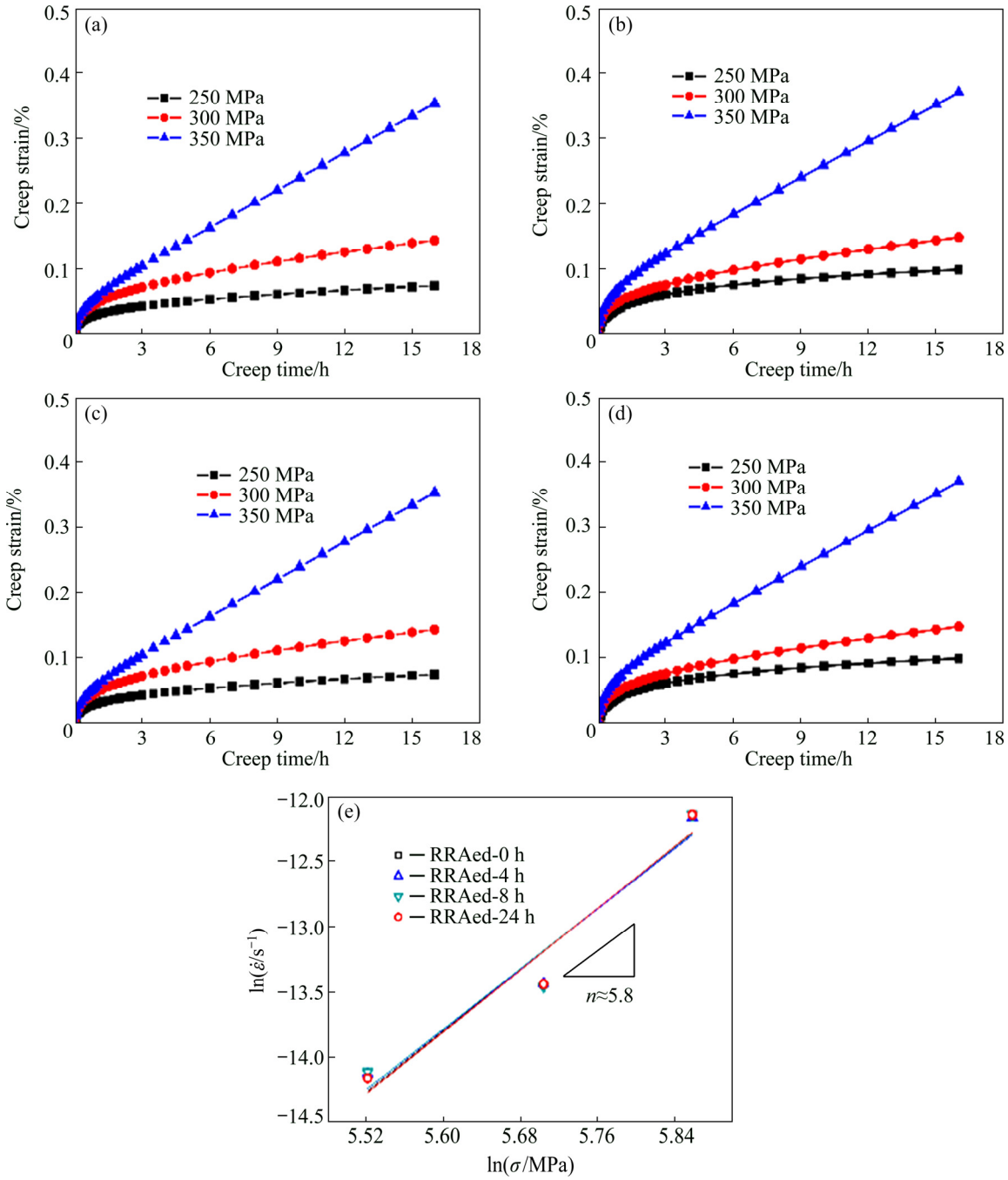

Fig. 4 Creep strain of RRAed-0 h (a), RRAed-4 h (b), RRAed-8 h (c) and RRAed-24 h (d) AA7150 samples, and stress exponent of different RRAed AA7150 samples (e)

re-aging time. This means that a suitable re-aging time should be selected for CAF application of AA7150. From the creep deformation of Fig. 3(a) and the mechanical properties of Fig. 6, 8 h of re-aging time may be a better choice to obtain coordinated regulation of precision and property of the CAF AA7150 components.

3.2.2 Electrical conductivity

Figure 7(a) shows the electrical conductivity of different RRAed AA7150 samples during the creep aging at 140 °C and 300 MPa. The effect of re-aging time on evolution of electrical conductivity is significant. The conductivity of RRAed-24 h sample is 1.6% IACS higher than that of the RRAed-0 h sample before creep aging. With the increase of re-aging time, the electrical conductivity of initial RRAed AA7150 samples is improved. The electrical conductivity of retrogression treated (RRAed-0 h) AA7150 increases with the increasing creep aging time. However, the electrical

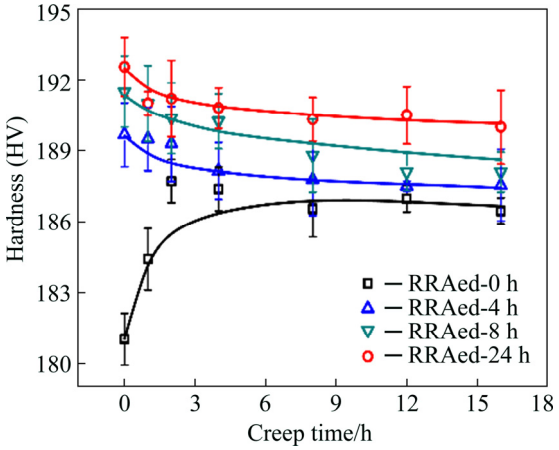

Fig. 5 Evolution of hardness of four different RRAed AA7150 samples during creep aging process

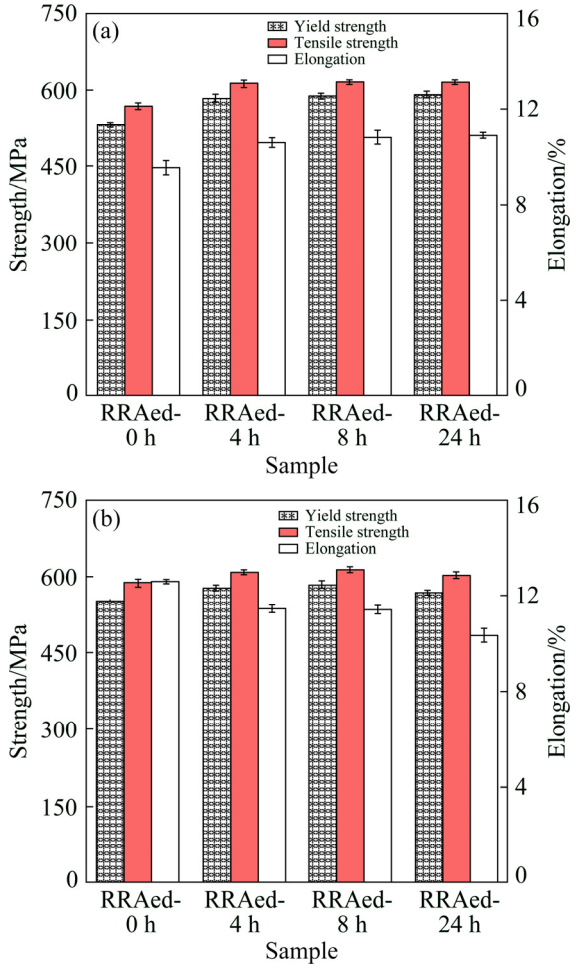

Fig. 6 Mechanical properties of four different RRAed AA7150 samples before (a) and after (b) creep aging process

conductivities of other three samples decrease first and then increase during the creep aging process. Compared Fig. 5 with Fig. 7(a), the trends of the

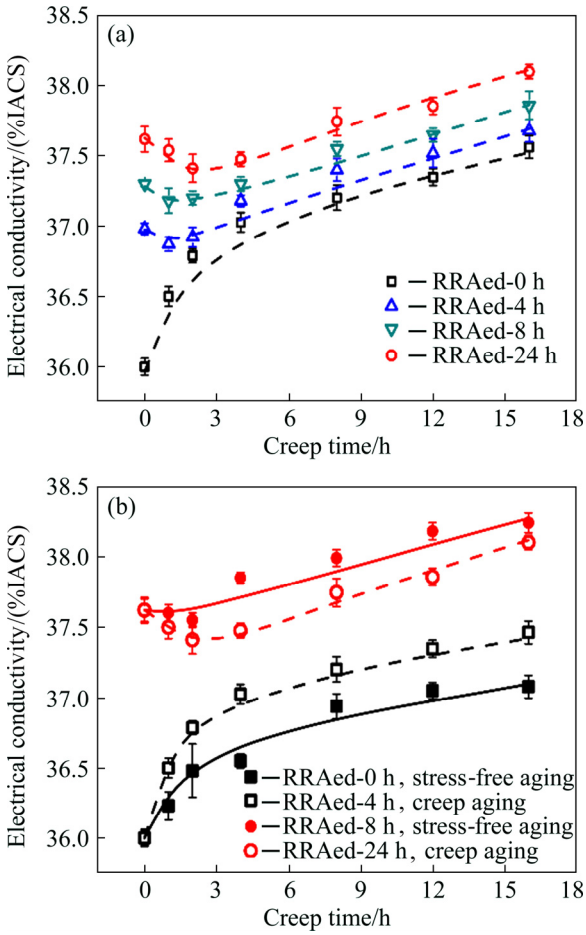

Fig. 7 Electrical conductivity evolution of different RRAed AA7150 samples at 140 °C: (a) Four different RRAed AA7150 samples during creep aging; (b) RRAed-0 h and RRAed-24 h samples during creep aging and stress-free aging respectively

hardness and conductivity of RRAed samples are similar during the primary creep aging process (less than 2 h). However, the trends are different after 2 h creep aging process. In the primary creep ageing process, the re-dissolution of the small precipitates (such as cluster and GP zones) is the main reason for the reduction of the hardness and conductivity in RRAed samples. With the increase of creep aging time, the precipitates continue to grow and even coarsen gradually. Therefore, the hardness decreases slowly due to the overaging of the 7150 aluminum alloy, whilst the conductivity is improved by the decrease in scattering centers. In order to further understand the effect of applied stress on the electrical conductivity of aged samples with various RRAed treatments, the electrical conductivities of RRAed-0 h and RRAed-24 h samples during the

creep aging (300 MPa) and stress-free aging at 140 °C are shown in Fig. 7(b). For RRAed-0 h sample, the electrical conductivity increases with the time in both creep aging and stress-free aging processes, and a large value is obtained by the former. Electrical conductivity can be served as an indicator of stress corrosion resistance of 7000 series aluminum alloys [18]. This shows that the applied stress can improve the electrical conductivity, which facilitates the stress corrosion resistance of CAF components. In addition, the electrical conductivity of RRAed-24 h sample first declines and then increases with the time in both creep aging and stress-free aging processes. The electrical conductivity of the creep-aged alloys is lower than that of stress-free aged alloys for RRAed-24 h sample. Also, the difference between two types of aging process in electrical conductivity is significant. But this kind of discrepancy decreases gradually after 4 h aging.

3.3 Precipitate microstructures before and after creep aging process of retrogression and re-aged AA7150

3.3.1 Grain interior and grain boundary precipitates before creep aging process

As generally accepted, in the re-aging process, the solute atoms dissolved in the Al matrix can re-precipitate and form new Guinier Preston zone (GP zone), and η' phase [19]. The final microstructures of RRA temper contain GP zone, η', η phases [19], and dense clusters [20]. Figure 8 shows the precipitates of three different AA7150 samples RRAed for 0, 8 and 24 h. Diffraction spots located at 1/3 and 2/3 of $(02\bar{2})_{Al}$ matrix reflection and streaks from $(\bar{1}1\bar{1})_{Al}$ and $(11\bar{1})_{Al}$ reflections are observed in the samples, compared with the diffraction characteristics of precipitates in other Al−Zn−Mg−Cu alloys [21,22]. This indicates that η' is the major precipitates at all samples. Figure 8(a) shows the morphology and distribution

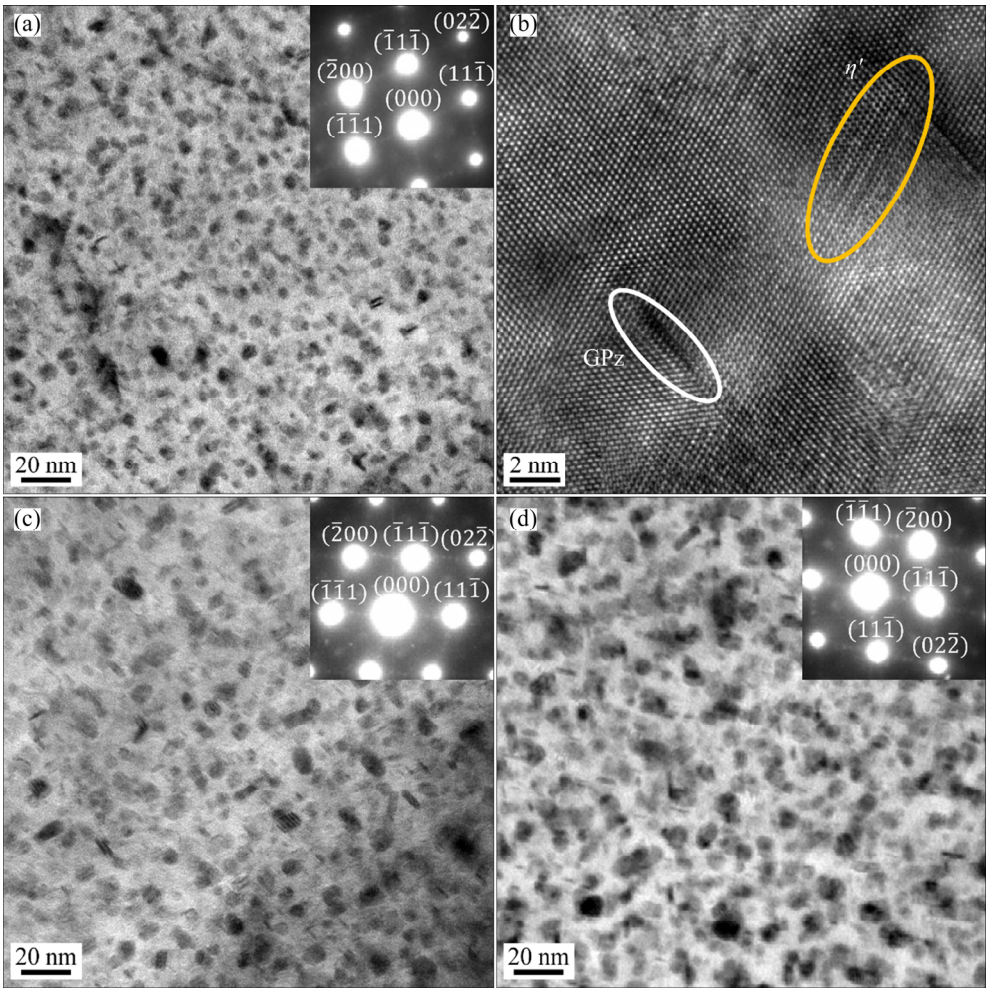

Fig. 8 TEM images of grain interior precipitates before creep aging process for different AA7150 samples (near ⟨011⟩Al direction): (a) RRAed-0 h; (b) HRTEM image of RRAed-0 h; (c) RRAed-8 h; (d) RRAed-24 h

of precipitates of RRAed-0h sample, and the corresponding HRTEM observation for RRAed-0h sample is shown in Fig. 8(b). It has been reported that the spherical GPI zone is coherent with the aluminum matrix with an average diameter of about 3 nm [23,24], and GPII zone is Zn-rich layers on $\{111\}_{Al}$ planes with 1−2 atomic layers in thickness and 3−5 nm in width [25,26]. HRTEM observation (Fig. 8(b)) reveals some fine GP zone (trapped in white circle) and a mature form of the η' phase (trapped in yellow circle). Figures 8(c) and (d) represent the grain interior precipitates of RRAed-8 h and RRAed-24 h samples, respectively. The abundant spherical precipitates are distributed homogeneously in the matrix, the average sizes of precipitates counted are about 6, 9 and 12 nm for RRAed-0 h, -8 h and -24 h samples, respectively. With the increase of re-aging time, the size of precipitates increases slightly.

Figure 9 refers to the grain boundary precipitates (GBPs) of AA7150 with three different RRAed samples of 0, 8 and 24 h. The precipitates of three different RRAed AA7150 samples are discontinuously distributed along the grain boundary and precipitates-free zone (PFZ) obviously exists. Existing research on grain boundary micro-structures shows that the growth and coarsening of grain boundary precipitates are accompanied by the formation of PFZ [27]. The formation and growth of PFZ can apparently reduce the mechanical properties of materials due to stress concentration near PFZ [28]. The discontinuous GBPs can improve corrosion resistance [29,30]. From Fig. 9, it can be seen that the re-aging process can promote the growth of the GBPs and increase the width of PFZ. This shows that as the re-aging time increases, the corrosion resistance of the AA7150 increases, but the mechanical properties may decrease.

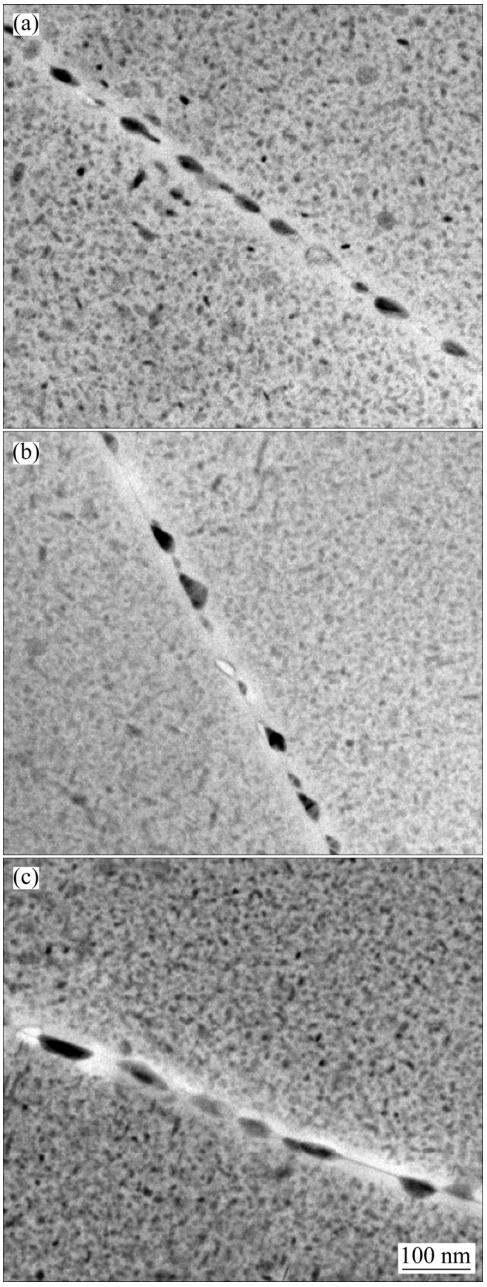

Fig. 9 TEM images of grain boundary precipitates before creep aging process for different RRAed AA7150 samples: (a) RRAed-0 h; (b) RRAed-8 h; (c) RRAed-24 h

3.3.2 Grain interior and grain boundary precipitates after creep aging process

The TEM images of the samples under different RRAed conditions after creep aging at 140 °C and 300 MPa are shown in Figs. 10(a)−(c), i.e., 0, 8, 24 h, respectively. From the $\langle 011\rangle_{Al}$ projection, the obvious diffraction spots at 1/3, 2/3 $(220)_{Al}$, 1/3 $(\bar{1}1\bar{1})_{Al}$ and $(11\bar{1})_{Al}$ indicate that η' phase is still the major precipitate after creep aging at 140 °C and 300 MPa for 16 h. Creep aging is actually a process of stress aging. It is known that the application of a stress during aging can significantly accelerate the aging process of alloys [31,32]. Compared with precipitation before creep aging, the grain interior precipitates are obviously coarsened and the amount is also reduced after creep aging. The average dimensions of the η' phase after creep aging are 10, 15 and 18 nm for the RRAed-0 h, -8 h and -24 h samples, respectively. With re-aging time of the initial samples increasing, the average size of the precipitates gradually rises

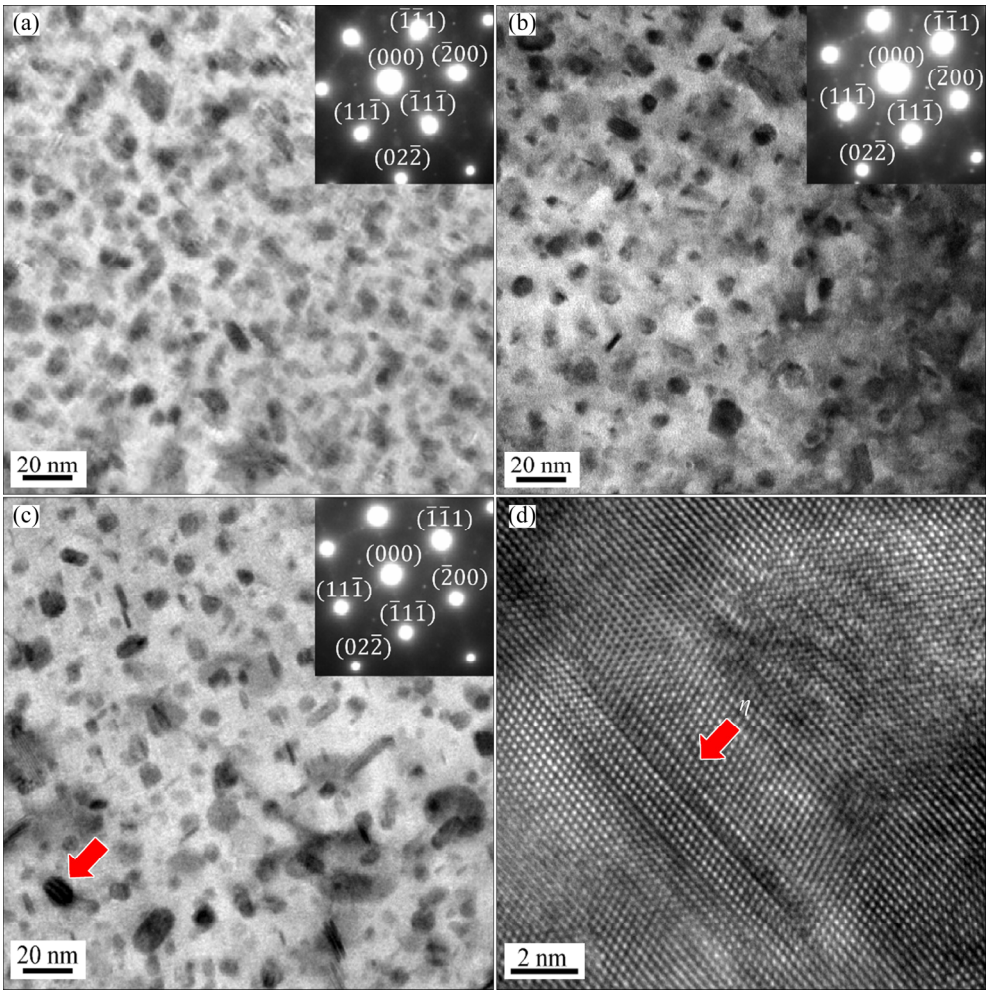

Fig. 10 TEM images of grain interior precipitates after creep aging process for different RRAed AA7150 samples (near $\langle 011 \rangle_{Al}$ direction): (a) RRAed-0 h; (b) RRAed-8 h; (c) RRAed-24 h; (d) HRTEM image of RRAed-24 h

after creep aging, but the density decreases. This indicates that the creep aging process mainly causes the coarsening of the precipitates, which is the large particles absorbing the small particles. Further, as shown in Fig. 10(c), some coarse precipitates about 30 nm appear, which are conformed as the stable η phase by a HRTEM image (Fig. 10(d)).

Figures 11(a)−(c) illustrate the GPBs patterns in three different RRAed AA7150 samples of 0, 8 and 24 h after creep aging at 140 °C and 300 MPa for 16 h. With the increase of the initial re-aging time, the precipitates of the grain boundary are coarser and more discontinuous after the creep aging. Comparing with the grain boundaries before creep aging, it can be seen that the stress promotes the growth of GBPs, and the size of precipitates increases probably by utilizing the elastic strain energy introduced by the applied stress during creep aging.

3.4 Relationship between macroscopic properties and microstructures during creep aging process of RRAed AA7150

3.4.1 Relationship between creep behavior and microstructures

The factors affecting the creep behavior mainly include grain structures, and grain interior/grain boundary microstructures. The creep aging temperature is much lower than the recrystallization temperature of the aluminum alloy, the grain texture and structures hardly change. Therefore, lattice distortion, dislocation density, grain interior precipitates morphology, distribution characteristics and grain boundary structures are main factors affecting the creep behavior of RRAed AA7150 samples in this work.

It can be seen from Figs. 3 and 4 that the steady creep rates and creep mechanism of different RRAed AA7150 samples are basically the same.

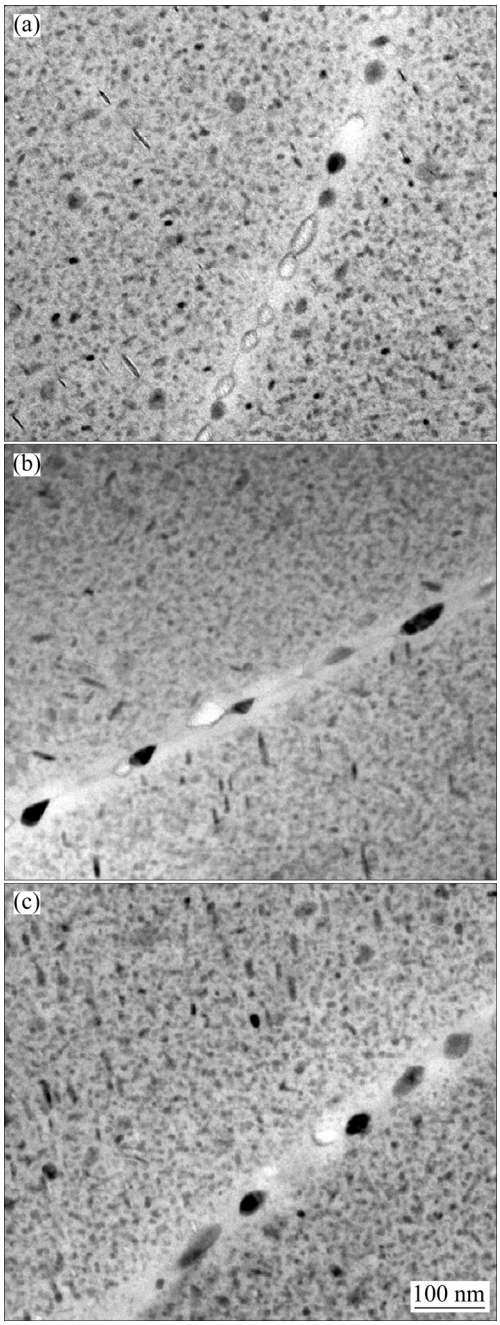

Fig. 11 TEM images of grain boundary precipitates after creep aging process for different RRAed AA7150 samples: (a) RRAed-0 h; (b) RRAed-8 h; (c) RRAed-24 h

However, the grain interior/grain boundary precipitates of different RRAed AA7150 samples are different (Figs. 8−11). With the increase of creep aging time, precipitates continuously nucleate, grow and coarsen. This indicates that the morphology and distribution of precipitates have no significant effect on the steady-state creep behavior of this alloy. From Fig. 3 and Table 1, the difference in creep behavior mainly comes from the primary creep stage. This is involved with the initial microstructures of the different RRAed AA7150 samples. Firstly, the samples with different re-aging time have undergone a long time of initial aging and retrogression process, and no significant difference in dislocation density and grain boundary structures exists. Therefore, dislocation density and grain boundary structures are not the reasons that affect the difference of the primary creep stage. With the increase of re-aging time, dissolving solute atoms re-precipitate, and the precipitate number and size increase slightly. At the same time, the lattice distortion caused by the dissolving atoms also decreases. It is generally believed that with the increase of the precipitate number, the more uniform the precipitate size and the finer the distribution are, the more obvious the obstacle to dislocation movement is, and the lower the creep deformation is performed. Lattice distortion is also a major factor hindering dislocation motion [33]. HO et al [34] studied the behavior of the initial creep stage and pointed out that the degree of solid solution was the main factor affecting the initial creep stage, and established a unified macro-micro creep constitutive model considering solution strengthening. In this work, the lattice distortion and precipitate structures caused by retrogression and re-aging process affect the initial creep stage together. However, the influence of lattice distortion is significantly higher than that of the precipitates. As the lattice distortion caused by retrogression decreases significantly after re-aging, the hindrance of lattice distortion to dislocation motion is weakened, the primary creep stages is prolonged, and the total creep is also increased.

3.4.2 Relationship between mechanical properties and microstructures

The material strength during the creep aging process is mainly composed of four parts: matrix strengthening, solution strengthening, precipitation strengthening and dislocation strengthening. Among them, the matrix strengthening is related to the grain structures and texture of the material, and does not change substantially. Before the creep aging, the material undergoes different re-aging processes at 120 °C, and the performance changes. As the re-aging time increases, the solution strengthening decreases gradually, the aging precipitation strengthening increases, and the dislocation does not change significantly.

Therefore, as the re-aging time increases, the strength and hardness increase (Fig. 5), which is mainly because the increase of precipitation strengthening is greater than the reduction of solid solution strengthening. In the creep aging process, the aging process is promoted by the stress at creep temperature of 140 °C, compared with the re-aging (temperature 120 °C and no stress) conditions, and the hardness of the retrogression temper (RRAed-0 h) sample first increases and then stabilizes. The increase in hardness can be attributed to the precipitation strengthening. However, the hardness of re-aged samples (RRAed-4 h, -8 h and -24 h) showed a monotonously reduced trend. The main reason is that the creep aging temperature is higher than the re-aging temperature, and the precipitates precipitated during the re-aging process are re-dissolved into the matrix to a certain extent. On one hand, the dissolved atoms are re-precipitated under high temperature and stress. On the other hand, the precipitates with a larger size continue to grow and coarsen, and enter the overage stage in advance, so the performance is mainly weakened. The lowest mechanical properties of the RRAed-24 h sample after the creep aging are also a good proof.

3.4.3 Relationship between electrical conductivity and microstructures

It is well known that the electrical resistance is caused by the conductive electron scattered by lattice distortion introduced by impurities, defects, and alloy elements [35,36]. A decrease in scattering centers leads to an increase in electrical conductivity. For aged alloy, according to the Mattiessen's rule, the total resistivity of the aged Al−Zn−Mg−Cu alloys can be expressed by [37,38]

$$\rho_{total}=\rho_0+\rho_{ss}+\rho_{dis}+\rho_{gb}+\rho_p \quad (1)$$

where ρ_{total} is the total electrical resistance of the alloy, ρ_0 is the intrinsic electrical resistivity of the lattice, ρ_{ss} is the resistivity due to solute atoms dissolved in the Al matrix, ρ_{dis} is the resistivity due to the dislocations, ρ_{gb} is the resistivity due to grain boundaries, and ρ_p is the resistivity induced by grain interior precipitates.

During the stress-free aging and creep aging process of RRAed-0 h sample, the increase of electrical conductivity is caused by the nucleation, growth and coarsening of aging precipitates. On one hand, the solution atoms are absorbed to form precipitates, resulting in reduction of lattice distortion induced by solid solution. On the other hand, the density of precipitates diminishes due to the coarsening of aging precipitates, which also improves the electron motion in the matrix. What's more, the grain boundary precipitates become more discontinuous during aging processes, which is also helpful to improve electrical conductivity. Thus, the electrical conductivity increases with the aging time. In addition, the applied stress promotes the aging precipitation process. Therefore, the electrical conductivity of RRAed-0 h sample in creep-aged alloys is higher than that in stress-free aged alloys.

For the electrical conductivity change of RRAed-24 h sample in both creep aging and stress-free aging process, it can also be related to changes in microstructures. Electrical conductivity decreases slightly at first and then rises gradually. It is speculated that after re-aging at 120 °C for 24 h, solute atoms have basically precipitated and grown up, and a few precipitates re-dissolve within 2 h when the temperature is raised to 140 °C, and then re-precipitate and grow up. In the RRAed-0 h sample, due to the previous high temperature retrogression, there are a large number of free solute atoms in Al matrix. Although there may be a small amount of dissolution due to temperature change, precipitation strengthening is the main process during aging process at 140 °C, so the electrical conductivity rises throughout the aging process. For the RRAed-24 h sample, the electrical conductivity decreases at first mainly by re-dissolution of fine precipitates, and the increase of electrical conductivity after aging at 140 °C for 4 h can be attributed to the coarsening of aging precipitates. As for the low electrical conductivity in creep aging process of RRAed-24 h sample, the reason could be that applied stress is also an energy field, like temperature, which causes more precipitates to dissolve back into the Al matrix [39]. Nevertheless, the applied stress is a double-edged sword. It can also promote the aging precipitation process. Thus, the difference between creep aging process and stress-free aging process in RRAed-24 h sample decreases after 4 h aging treatment.

4 Conclusions

(1) With the increases of re-aging time, the grain interior and boundary precipitates become coarser and more discontinuous, and the PFZ also becomes wider. After the creep aging process, the grain interior and boundary precipitates of different RRAed alloys are further coarsened and the PFZ is broadened.

(2) The total creep strain increases over the re-aging time, which is beneficial to improving the creep ageing formability. What's more, re-aging process mainly affects the dislocation motion during the primary creep stage. But the effect on the steady-state creep rate is not obvious. The stress exponent indicates that the creep mechanism of different re-aged samples is dominated by dislocation climb.

(3) Re-aging process is beneficial to increasing the hardness and electrical conductivity during creep aging process. This means that the retrogression and re-aging treatment can improve the forming efficiency and stress corrosion resistance of CAF components. However, elongation of the creep aged AA7150 declines when the re-aging time exceeds 24 h. Therefore, a suitable re-aging time should be selected to obtain the best comprehensive performance of the CAF components.

References

[1] LIAO Bin, WU Xiao-dong, YAN Chang-jian, LIU Zheng, JI Yan-li, CAO Ling-fei, HUANG Guang-jie, LIU Qing. Microstructure characterization of Al-cladded Al−Zn−Mg−Cu sheet in different hot deformation conditions [J]. Transactions of Nonferrous Metals Society of China, 2017, 27(8): 1689−1697.

[2] LI Hong-ying, LIU Jiao-jiao, YU Wei-chen, ZHAO Hui, LI De-wang. Microstructure evolution of Al−Zn−Mg−Cu alloy during non-linear cooling process [J]. Transactions of Nonferrous Metals Society of China, 2016, 26(5): 1191−1200.

[3] XU Yong-qian, ZHAN Li-hua, HUANG Ming-hui, SHEN Rui-Lin, MA Zi-yao, XU Ling-zhi, WANG Kai, WANG Xun. Deformation behavior of Al−Cu−Mg alloy during non-isothermal creep age forming process [J]. Journal of Materials Processing Technology, 2018, 255: 26−34.

[4] YANG You-liang, ZHAN Li-hua, SHEN Ru-lin, LIU Jian, LI Xi-cai, HUANG Ming-hui, HE Di-qiu, CHANG Zhi-long, MA Yun-long, WAN Li. Investigation on the creep-age forming of an integrally-stiffened AA2219 alloy plate: Experiment and modeling [J]. International Journal of Advanced Manufacturing Technology, 2018, 95: 2015−2025.

[5] LI J F, BIRBILIS N, LI C X, JIA Z Q, CAI B, ZHENG Z Q. Influence of retrogression temperature and time on the mechanical properties and exfoliation corrosion behavior of aluminium alloy AA7150 [J]. Materials Characterization, 2009, 60(11): 1334−1341.

[6] ANGAPPAN M, SAMPATH V, ASHOK B, DEEPKUMAR V P. Retrogression and re-aging treatment on short transverse tensile properties of 7010 aluminium alloy extrusions [J]. Materials and Design, 2011, 32(7): 4050−4053.

[7] ARABI JESHVAGHANI R, EMAMI M, SHAHVERDI H R, HADAVI S M M. Effects of time and temperature on the creep forming of 7075 aluminum alloy: Springback and mechanical properties [J]. Materials Science and Engineering A, 2011, 528(29−30): 8795−8799.

[8] ARABI JESHVAGHANI R, SHAHVERDI H R, HADAVI S M M. Investigation of the age hardening and operative deformation mechanism of 7075 aluminum alloy under creep forming [J]. Materials Science and Engineering A, 2012, 552: 172−178.

[9] ZHAN L H, LIN J G, DEAN T A, HUANG M H. Experimental studies and constitutive modelling of the hardening of aluminium alloy 7055 under creep age forming conditions [J]. International Journal of Mechanical Sciences, 2011, 53(8): 595−605.

[10] ZHANG Jin, WANG Yu, DENG Yun-lai, ZHANG Xin-ming. Effect of deformation degree on the creep age forming of 7475 aluminum alloy: The feasibility of the extended deformation range [J]. Materials Science and Engineering A, 2016, 664: 126−134.

[11] LIN Y C, ZHANG J L, CHEN M S. Evolution of precipitates during two-stage stress-aging of an Al−Zn−Mg−Cu alloy [J]. Journal of Alloys and Compounds, 2016, 684: 177−187.

[12] ZHENG Jing-hua, PAN Ran, LI Chen, ZHANG Wei, LIN Jian-guo, DAVIES C M. Experimental investigation of multi-step stress-relaxation-ageing of 7050 aluminium alloy for different pre-strained conditions [J]. Materials Science and Engineering A, 2018, 710: 111−120.

[13] ARABI JESHVAGHANI R, ZOHDI H, SHAHVERDI H R, BOZORG M, HADAVI S M M. Influence of multi-step heat treatments in creep age forming of 7075 aluminum alloy: Optimization for springback, strength and exfoliation corrosion [J]. Materials Characterization, 2012, 73: 8−15.

[14] LEI C, YANG H, LI H, SHI N, ZHAN L H. Dependences of microstructures and properties on initial tempers of creep aged 7050 aluminum alloy [J]. Journal of Materials Processing Technology, 2017, 239: 125−132.

[15] XU Yong-qian, ZHAN Li-hua, LI Shu-jian, WU Xin-tong. Effect of stress-aging treatments on precipitates of pre-retrogressed Al−Zn−Mg−Cu alloy [J]. Rare Metal Materials and Engineering, 2017, 46(2): 355−362.

[16] CHEN J F, JIANG J T, ZHEN L, SHAO W Z. Stress relaxation behavior of an Al−Zn−Mg−Cu alloy in simulated age-forming process [J]. Journal of Materials Processing Technology, 2014, 214(4): 775−783.

[17] YANG You-liang, ZHAN Li-hua, LIU Chun-hui, WANG Xun, WANG Qing, TANG Zhi-mao, LI Guo-peng, HUANG Ming-hui, HU Zheng-gen. Stress-relaxation ageing behavior

and microstructural evolution under varying initial stresses in an Al−Cu alloy: Experiments and modeling[J]. International Journal of Plasticity, 2020, 127: 102646.

[18] LEI C, LI H, ZHENG G W, FU J. Thermal-mechanical loading sequences related creep aging behaviors of 7050 aluminum alloy [J]. Journal of Alloys and Compounds, 2018, 731: 90−99.

[19] AZARNIYA A, TAHERI A K, TAHERI K K. Recent advances in ageing of 7xxx series aluminum alloys: A physical metallurgy perspective [J]. Journal of Alloys and Compounds, 2019, 781: 945−983.

[20] MARLAUD T, DESCHAMPS A, BLEY F, LEFEBVRE W, BAROUX B. Evolution of precipitate microstructures during the retrogression and re-ageing heat treatment of an Al−Zn−Mg−Cu alloy [J]. Acta Materialia, 2010, 58: 4814−4826.

[21] LIU Fei, BAI Pu-cun, HOU Xiao-hu, TONG Nai-qiang, CUI Xiao-ming. Transmission electron microscopic observation of a novel Al_3Zr-η' core-shell particle in Al−Zn−Mg−Cu alloy [J]. Rare Metal Materials and Engineering, 2018, 47(11): 3272−3276.

[22] WEI Li-jun, HAN Bao-shuai, YE Fan, DITTA A, LI Long, XU Yan-jin, WU Su-jun. Influencing mechanisms of heat treatments on microstructure and comprehensive properties of Al−Zn−Mg−Cu alloy formed by spray forming [J]. Journal of Materials Research and Technology, 2020, 9(3): 6850−6858.

[23] WANG Feng, XIONG Bai-qing, ZHANG Yong-an, ZHU Bao-hong, LIU Hong-wei, HE Xiao-qing. Effect of heat treatment on the microstructure and mechanical properties of the spray-deposited Al−10.8Zn−2.8Mg−1.9Cu alloy [J]. Materials Science and Engineering A, 2008, 486(1−2): 648−652.

[24] ZHANG Miao, LIU Tao, HE Chun-nian, DING Jian, LIU En-zuo, SHI Chun-sheng, LI Jia-jun, ZHAO Nai-qin. Evolution of microstructure and properties of Al−Zn−Mg−Cu−Sc−Zr alloy during aging treatment [J]. Journal of Alloys and Compounds, 2016, 658: 946−951.

[25] GUO Wei, GUO Ji-yan, WANG Jin-duo, YANG Meng, LI Hui, WEN Xi-yu, ZHANG Jing-wu. Evolution of precipitate microstructure during stress aging of an Al−Zn−Mg−Cu alloy [J]. Materials Science and Engineering A, 2015, 634: 167−175.

[26] BUHA J, LUMLEY R N, CROSKY A G. Secondary ageing in an aluminium alloy 7050 [J]. Materials Science and Engineering A, 2008, 492(1−2): 1−10.

[27] LIN Y C, JIANG Yu-qiang, CHEN Xiao-ming, WEN Dong-xu, ZHOU Hua-min. Effect of creep-aging on precipitates of 7075 aluminum alloy [J]. Materials Science and Engineering A, 2013, 588: 347−356.

[28] CAI B, ADAMS B, NELSON T. Relation between precipitate-free zone width and grain boundary type in 7075-T7 Al alloy [J]. Acta Materialia, 2007, 55(5): 1543−1553.

[29] MARLAUD T, MALKI B, DESCHAMPS A, BAROUX B. Electrochemical aspects of exfoliation corrosion of aluminium alloys: The effects of heat treatment [J]. Corrosion Science, 2011, 53(4): 1394−1400.

[30] LIN Y C, PENG Xiao-bin, JIANG Yu-qiang, SHUAI Ci-jun. Effects of creep-aging parameters on aging precipitates of a two-stage creep-aged Al−Zn−Mg−Cu alloy under the extra compressive stress [J]. Journal of Alloys and Compounds, 2018, 743: 448−455.

[31] LIU Xiao-yan, PAN Qing-lin, ZHANG Xi-liang, LIANG Shun-xing, ZHENG Li-yun, GAO Fei, XIE Hai-long. Effects of stress-aging on the microstructure and properties of an aging forming Al−Cu−Mg−Ag alloy [J]. Materials and Design, 2014, 58: 247−251.

[32] GUO Wei, STEINBACH I, SOMSEN C, EGGELER G. On the effect of superimposed external stresses on the nucleation and growth of Ni_4Ti_3 particles: A parametric phase field study [J]. Acta Materialia, 2011, 59(8): 3287−3296.

[33] WANG Peng, WU Yuan, LIU Jia-bin, WANG Hong-tao. Impacts of atomic scale lattice distortion on dislocation activity in high-entropy alloys [J]. Extreme Mechanics Letters, 2017, 17: 38−42.

[34] HO K C, LIN J, DEAN T A. Constitutive modelling of primary creep for age forming an aluminium alloy [J]. Journal of Materials Processing Technology, 2004, 153−154: 122−127.

[35] SUN Yi-shan, JIANG Fu-lin, ZHANG Hui, SU Jian, YUAN Wu-han. Residual stress relief in Al−Zn−Mg−Cu alloy by a new multistage interrupted artificial aging treatment [J]. Materials and Design, 2016, 92: 281−287.

[36] LIN Hua-qiang, YE Ling-ying, SUN Lin, XIAO Tao, LIU Sheng-dan, DENG Yun-lai, ZHANG Xin-ming. Effect of three-step homogenization on microstructure and properties of 7N01 aluminum alloys [J]. Transactions of Nonferrous Metals Society of China, 2018, 28(5): 829−838.

[37] MURASHKIN M Y, SABIROV I, SAUVAGE X, VALIEV R Z. Nanostructured Al and Cu alloys with superior strength and electrical conductivity [J]. Journal of Materials Science, 2015, 51(1): 33−49.

[38] JIANG Sheng-yu, WANG Rui-hong, Grain size-dependent Mg/Si ratio effect on the microstructure and mechanical/ electrical properties of Al−Mg−Si−Sc alloys [J]. Journal of Materials Science & Technology, 2019, 35(7): 1354−1363.

[39] FAN Cai-he, OU Ling, HU Ze-yi, YANG Jian-jun, CHEN Xi-hong. Re-dissolution and re-precipitation behavior of nano-precipitated phase in Al−Cu−Mg alloy subjected to rapid cold stamping [J]. Transactions of Nonferrous Metals Society of China, 2019, 29(12): 2455−2462.

回归再时效 7150 铝合金的蠕变时效行为

王 庆[1,2]，湛利华[1,2,3]，徐永谦[1,2,3]，刘春辉[1,2]，赵 兴[1,2]，徐凌志[1,2]，杨有良[1,2]，蔡一贤[1,2,3]

1. 中南大学 机电工程学院，长沙 410083；
2. 中南大学 高性能复杂制造国家重点实验室，长沙 410083；
3. 中南大学 轻合金研究院，长沙 410083

摘 要：通过蠕变时效实验、拉伸性能测试、电导率测试和透射电镜观察，系统研究回归再时效状态的 7150 铝合金的蠕变时效行为。蠕变时效实验结果表明，回归再时效状态 7150 铝合金的稳态蠕变主要是位错攀移机制(应力指数≈5.8)，其稳态蠕变行为对晶内和晶界的析出相变化不敏感，但总的蠕变变形随着再时效时间的延长而增大。另外，在 140 °C 蠕变时效 16 h 后，4 种回归再时效样品的屈服强度和抗拉强度基本相同，但伸长率随着再时效时间的延长略有下降。而且回归再时效处理有利于提高 7150 铝合金的硬度和电导率。研究结果表明，蠕变时效前的回归再时效处理可以改善 7150 铝合金的晶内和晶界组织，提高合金的成形效率，改善合金的综合性能，包括力学性能和电导率。

关键词：蠕变时效成形；蠕变行为；力学性能；电导率；时效析出相；Al−Zn−Mg−Cu 合金

(Edited by Xiang-qun LI)